Intermediate-Field de Haas–van Alphen Effect in Zinc*

R. J. Higgins,† J. A. Marcus, and D. H. Whitmore

Northwestern University, Evanston, Illinois

(Received 27 July 1964; revised manuscript received 1 October 1964)

Torsion measurements have been made of the de Haas–van Alphen oscillations in zinc in magnetic fields up to 33 kG, using time-differentiation techniques to extract the higher frequency oscillations from a much larger background of low-frequency oscillations. In addition to the six frequencies observed by earlier investigators, seven new frequencies were observed in the frequency range 10^7–10^8 G. Six of these can be assigned to orbits on the nearly-free-electron Fermi surface model, confirming the validity of the model for some of the larger orbits on the Fermi surface. A frequency of $73._5 \times 10^6$ G has been assigned to the third band lens, and is only 4% smaller than predicted by the model for $H \perp [0001]$. Three other frequencies can be assigned to orbits on the multiply connected second-band section, two of which have alternative assignments involving magnetic breakdown of the spin-orbit energy gap. Frequencies of 12×10^6 and 17×10^6 G observed for H near $[0001]$ suggest assignment to the fourth-band cigar and third-band butterflies, though the dominance of other frequencies prevented the determination of the orientation dependence. A frequency of 47×10^6 G observed for H in the (0001) plane has not been assigned to the model Fermi surface.

INTRODUCTION

MANY physical properties of high-purity metals at temperatures near 0°K are oscillatory functions of applied magnetic field H.[1] In particular, the de Haas–van Alphen (dHvA) oscillations in magnetic susceptibility are periodic in $1/H$, the period being inversely proportional to the extremal cross-sectional area A of the Fermi surface (FS) normal to the magnetic field direction. The dHvA frequency F is given by the Onsager[2]-Lifshitz[3] relation:

$$F = (c/2\hbar\pi e)A = (1.045 \times 10^8)A \qquad (1)$$

[F in gauss, A in k-space units $(2\pi/\text{Å})^2$]. Thus the measurement of dHvA frequencies as a function of magnetic-field direction (relative to crystallographic directions) can be of great utility in experimental determination of the FS of metals. The complicated spectrum of dHvA frequencies observed in polyvalent metals can often be interpreted with the aid of the nearly free-electron (NFE) construction of Harrison.[4] However, unless the orientation dependence of frequencies can be carefully determined their assignment to the nearly-free-electron Fermi surface (NFEFS) can be ambiguous, owing to the multiplicity of extremal areas on the NFEFS. Also, it has recently become apparent that the appropriateness of the NFEFS depends on the magnitude of the applied magnetic field, because

of the phenomenon of magnetic breakdown (quantum-mechanical tunneling through small-band gaps).[5–7]

The NFEFS for zinc[8] is shown in Fig. 1, in the single-zone scheme appropriate to spin-orbit splitting of the degeneracy across the (0001) zone face.[9] The surface consists of hole-pockets in the first band; a multiply connected hole surface in the second band (often referred to as the "monster"); small "needles" along the vertical edges, a large disk, or "lens" in the center, and partial disks (which remap to form four-winged "butterflies") in the third band; and electron segments or "cigars" in the fourth band. Without spin-orbit coupling, the double-zone scheme is more appropriate (as illustrated in Ref. 4). In this case, the cigars and butterflies remap to form partially open "clamshells." The
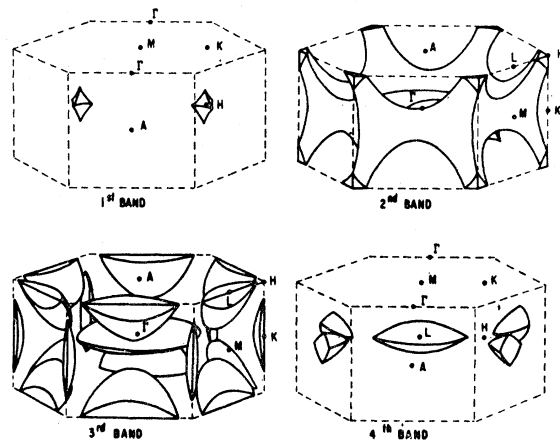

FIG. 1. The nearly free-electron Fermi surface for zinc (drawing taken from Ref. 8).

[1] See, for example, *The Fermi Surface*, edited by W. A. Harrison and M. B. Webb (John Wiley & Sons, New York, 1960).

[2] L. Onsager, Phil. Mag. 43, 1006 (1952).

[3] I. M. Lifshitz and A. N. Kosevich, Zh. Eksperim. i Teor. Fiz. 29, 730 (1955) [English transl.: Soviet Physics JETP 2, 636 (1956)].

[4] W. A. Harrison, Phys. Rev. 118, 1190 (1960).

[5] Morrel H. Cohen and L. Falicov, Phys. Rev. Letters 7, 231 (1961).

[6] E. I. Blount, Phys. Rev. 126, 1636 (1962).

[7] A. B. Pippard, Proc. Roy. Soc. (London) A270, 1 (1962).

[8] W. A. Harrison, Phys. Rev. 126, 497 (1962).

[9] L. M. Falicov and Morrel H. Cohen, Phys. Rev. 130, 92 (1963).

first-band pockets remap onto the monster at the point H, and the monster is no longer connected along the [0001] direction in the extended zone scheme, although monsters from three adjacent zones still come together along the HK line. The lens and needles are the same in both single and double zone schemes.

Six dHvA periods were observed in zinc by Joseph and Gordon[10] (JG) and correspond well to the NFEFS extremal area of the needle and to three extremal areas on the monster present in both zone schemes. It was suggested that beats observed in one of the oscillations were due to orbits on the first band pockets and the monster junction at H, evidence for the single-zone scheme. Magnetoresistance measurements[11,12] indicate open orbits along [0001] at low fields, changing to closed orbits above[12] 17.5 kG as the spin-orbit energy gap suffers magnetic breakdown, changing the connectivity of the monster from that of a single zone to that of the double zone. However, the recent observation of a large area dHvA oscillation assignable only to the single zone suggests that [0001] magnetic breakdown is not complete even at[13] 100 kG. Magnetic breakdown also occurs on the needle (similar to that observed in magnesium[14]), as observed in magnetoresistance,[11,12] in the anomalously large de Haas–Schubnikov conductivity oscillations,[15] the anomalously small dHvA oscillations,[16–18] and in the observation of an orbit corresponding to the free-electron sphere.[19]

The present measurements were an attempt to observe in magnetic fields up to 33 kG some of the larger orbits on the NFEFS not observed by JG in fields up to 23 kG, and to look for signs of the transition from single- to double-zone scheme as the magnetic field is raised above the breakdown field. Preliminary measurements showed traces of high frequency oscillations which were nearly obscured by large-amplitude low-frequency oscillations. Electronic analog differentiation was used to suppress the relative amplitude of low-frequency oscillations, and resulted in the observation of seven frequencies in addition to the six observed by JG.

[10] A. S. Joseph and W. L. Gordon, Phys. Rev. 126, 489 (1962). This paper gives reference to earlier dHvA measurements on zinc.

[11] W. A. Reed and G. F. Brennert, Phys. Rev. 130, 565 (1962).

[12] R. W. Stark, Phys. Rev. 135, A1698 (1964).

[13] M. G. Priestley and M. Mondino, Bull. Am. Phys. Soc. 9, 551 (1964).

[14] M. G. Priestley, Proc. Roy Soc. (London) A276, 258 (1963).

[15] R. W. Stark, Phys. Rev. Letters, 9, 482 (1962).

[16] J. S. Dhillon and D. Shoenberg, Phil. Trans. Roy. Soc. A248, 1 (1955).

[17] J. R. Lawson and W. L. Gordon, in Proceedings of the Ninth International Conference on Low Temperature Physics, 1964 (Plenum Press, New York, 1965).

[18] R. J. Higgins, J. A. Marcus and D. H. Whitmore, Proceedings of the Ninth International Conference on Low Temp. Physics, 1964 (Plenum Press, New York, 1965).

[19] A. C. Thorsen, in Proceedings of the Ninth International Conference on Low Temperature Physics, 1964 (Plenum Press, New York, 1965).

EXPERIMENTAL PROCEDURE

Sample Preparation

The zone-refined zinc crystal used in this research had a residual resistance ratio of 35 000.[20] The crystal was cut into roughly spherical samples weighing 100 mg with an acid string saw using concentrated hydrochloric acid and Teflon thread.[21] The crystals were then x-ray oriented using the back reflection Laue technique and epoxy cemented to 1 mm quartz rods, 6 cm long, which defined the torsion axes. Samples were prepared with torsion axes within 1° of the [0001], [10$\bar{1}$0], and [11$\bar{2}$0] crystallographic directions.

Magnetic Field

An ADL 11-in. iron core electromagnet was used with poles tapered to 3 in. and a 1 in. gap producing a magnetic field up to 33 kG. Both magnet current and magnet angle were motor-driven, allowing continuous recording of dHvA oscillations in $1/H$ at fixed angle and oscillations at fixed $1/H$ as a function of angle. Magnetic field strength was measured with a Siemens FC-34 high-linearity Hall probe. The Hall probe was driven by a dc analog divider circuit[22] whose output (the Hall current) was proportional to the inverse of the magnetic field strength. The Hall current was sampled across a 1-Ω resistor and, suitably attenuated, fed to the x axis of a Mosely Type 2-S xy recorder. The dHvA oscillations were thus recorded directly as a function of $1/H$. A zero-suppression circuit and a variable sensitivity setting made it possible to display a small interval of $1/H$ across the x-axis of the recorder (typically 307 to 345 $\times 10^{-7}$ G^{-1} over 38 cm). The $1/H$ sensitivity scale was chosen to give at least 100 to 200 oscillations across the x axis in order to make frequency determination as precise as possible.

Torque Measurements

Magnetic torque was measured with a feedback torsion balance designed and built by J. H. Condon, and described earlier.[23] The experimental arrangement is shown in Fig. 2. The sample was immersed in a bath of liquid helium. By pumping on the bath the temperature could be lowered to 1.2°K. Most measurements were made at this lowest temperature to enhance the amplitude of the oscillations. The circuitry on the right-hand side of Fig. 2 provides a means of separating high-frequency oscillations from a background of low-frequency oscillations much larger in amplitude. By varying the

[20] The zinc was zone refined by J. H. Wernick and crystals were grown by P. R. Schmidt at the Bell Telephone Laboratories. Samples from this same lot were used in the magnetoresistance measurements of W. A. Reed (Ref. 11) and the magnetoacoustic attenuation investigation of Gibbons and Falicov (Ref. 32).

[21] Teflon thread (Premier Thread Company, Bristol, R. I.) made a considerable improvement in smoothness of cutting and acid carrying ability over the usual Saran monofilament.

[22] R. J. Higgins, Rev. Sci. Instr. (to be published).

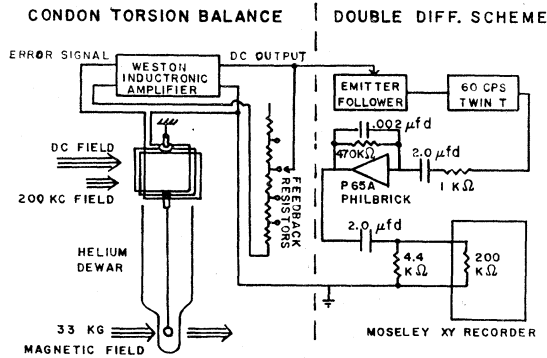[23] J. H. Condon and J. A. Marcus, Phys. Rev. 134, A446 (1964).

FIG. 2. Magnetic torque measurement. Left: the electronic feedback torsion balance (see footnote 23). Right: time differentiation technique for enhancing the amplitude of high-frequency oscillations (the field-dependent oscillations are made time-dependent by sweeping the 30-kG magnetic field).

magnet current linearly in time, dHvA oscillations are made time-dependent,[24] and can be selectively amplified by standard analog computer techniques.[25] High-frequency oscillations are emphasized by differentiation, which multiplies the amplitude of each oscillation by its frequency. The dc amplifier-feedback circuit shown in Fig. 2 has a transfer function:

$$\frac{E_{out}}{E_{in}} = \frac{RCs}{(1+R'Cs)(1+RC's)}, \tag{2}$$

where $s = 2\pi iF$, $C = 2.0 \ \mu F$, $R = 470 \ k\Omega$, $C' = 0.002 \ \mu F$, and $R' = k\Omega$. At typical signal frequencies, the circuit acts very nearly as an ideal differentiator, $E_{out}/E_{in} \simeq RCs$. Unwanted noise at higher frequencies is attenuated, since the transfer function varies as $1/s$ at high frequencies. A second stage of differentiation is provided by a passive filter between the active differentiator and the y-axis of the recorder.

A trace of fine structure in recorded dHvA oscillations (Fig. 3, bottom; the fine structure is too small to be seen in this reproduction) is well resolved by differentiation and expansion of the $1/H$ scale (Fig. 3, middle). A trace of additional high-field fine structure (Fig. 3, middle, left) is resolved (Fig. 3, top) by a second stage of differentiation and additional scale expansion.

EXPERIMENTAL RESULTS

The spectrum of dHvA frequencies measured in the three symmetry planes is shown in Fig. 4, (0001), Fig. 5, (10$\bar{1}$0), and Fig. 6, (11$\bar{2}$0), as a function of magnetic field direction. There are two lower frequencies

---

[24] Since $1/H$ does not vary linearly in time, the dHvA oscillations are not periodic in time. Differentiated amplitudes are multiplied by $[d(1/H)/dI][dI/dt]$, where I is the magnet current. This term affects oscillation amplitude but dHvA frequency is unaffected.

[25] A. S. Jackson, *Analog Computation* (McGraw-Hill Book Company, Inc., New York, 1960). Similar techniques have recently been used by other investigators; for example, A. S. Joseph and A. C. Thorsen, Phys. Rev. **133**, A1546 (1964).
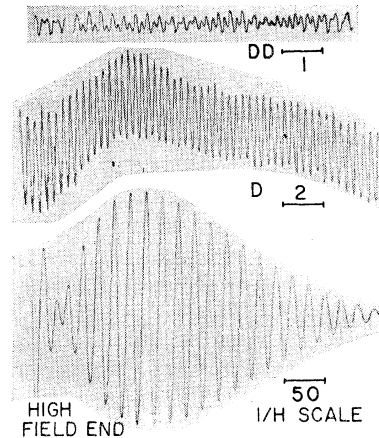

FIG. 3. Torque oscillations as a function of $1/H$ showing the high-frequency fine structure revealed by time differentiation. Bottom: undifferentiated. Middle: singly differentiated, $1/H$ scale expanded by a factor of 25. Top: doubly differentiated, $1/H$ scale expanded by an additional factor of 2. $1/H$ scales shown are in units of $10^{-7} \ G^{-1}$. One cycle of oscillation on the bottom curve covers the full width of the middle curve and twice the width of the upper curve.

which are not plotted, since these have been discussed adequately by JG. The indexing of frequencies follows the notation of JG, who labeled their observed periods P_1 to P_6. The additional frequencies presented are labeled F_7 to F_{13}. Except for F_7 and F_8, the indexing is in order of increasing frequency. F_3 actually consists of several beating frequencies, the lowest of which is shown in Figs. 5 and 6. The other branches of F_3 are discussed fully by JG. Frequency F_3 reaches a minimum about 30° from [0001]. At this angle, our value is 1% lower than JG in the (10$\bar{1}$0) plane and 2% higher in the (11$\bar{2}$0) plane.

Before considering each of the high-frequency oscillations, mention should be made of the limiting precision of frequency determination due to counting errors. Frequencies F_9, F_{13}, and, in the (11$\bar{2}$0) plane, F_6, can be most precisely determined since they are clearly distinguishable from other oscillations at a given angle. Several hundred oscillations were counted in a given field sweep, so that the limiting precision due to counting errors is several parts in 10^3. However, other sources of error, such as the sensitivity of the Hall-probe voltage to the ambient temperature, limit the reproducibility of these frequencies to about $\pm 1/2\%$. A second group of frequencies, labeled F_{11}, F_{12}, and, in the (10$\bar{1}$0) plane, F_6, are small in amplitude compared with other oscillations; there may be a counting error of 1 or 2 oscillations in 50. The uncertainty is typically ± 2 to 4%. Finally, frequencies, F_7, F_8, and F_{10} are very nearly hidden by F_3 and are resolvable only at a few angles. These frequencies are determined only to $\pm 10\%$.

F_9 in the (0001) Plane

For magnetic fields in the (0001) plane near [1$\bar{2}$10] (Fig. 4), F_9 has a minimum frequency of 26.6×10^6 G
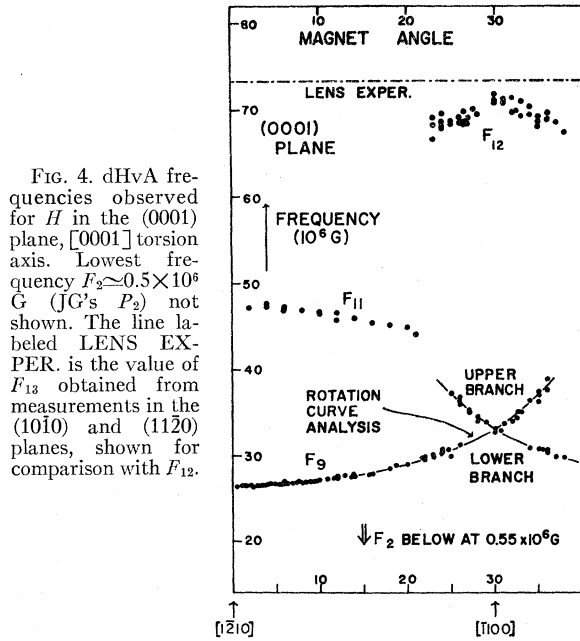
FIG. 4. dHvA frequencies observed for H in the (0001) plane, [0001] torsion axis. Lowest frequency $F_2 \simeq 0.5 \times 10^6$ G (JG's P_2) not shown. The line labeled LENS EXPER. is the value of F_{13} obtained from measurements in the (10$\bar{1}$0) and (11$\bar{2}$0) planes, shown for comparison with F_{12}.

$\pm 1\%$, corresponding to a FS area of 0.25_4Å^{-2}. At [$\bar{1}$100] $F = 33._0 \times 10^6$ G, corresponding to an area of 0.31_5Å^{-2}. Care has been taken to verify the crossing of symmetrically oriented curves at [$\bar{1}$100], as this detail affects our interpretation of the number and shape of the Fermi surface pieces responsible for the oscillations. However, because of frequency modulation effects[26] near [$\bar{1}$100] the crossing could not be verified reliably by reducing the beat structure of field sweep oscillations. As an alternative technique, the crossing has been verified by following frequency changes via "angular" dHvA oscillations.[27] That is, by keeping the magnetic field constant in magnitude but steadily rotating its

---

[26] The amplitude modulated beat structure of F_9 within 6° of [1$\bar{1}$00] was complicated by additional frequency modulation (FM). The local frequency of F_9 oscillates above and below the average with an amplitude typically 10% and a period just equal to that of the large amplitude low frequency oscillation P_2. Similar coupling effects have been reported by other investigators [e.g.: D. Shoenberg, Phil. Trans. Roy Soc. A255, 85 (1962), and N. F. Brandt, T. F. Dolgolenko, and N. N. Stupochenko, Zh. Eksperim. i Teor. Fiz. 45, 1319 (1963) [English transl.: Soviet Physics—JETP 18, 908 (1964)] with the suggestion that the coupling may be due to the replacement of H by B in the Lifshitz formula (Ref. 3). However, the present observations can be satisfactorily explained by a slight twisting of the crystal under the influence of the large oscillatory torque P_2, causing apparent frequency modulation as the field is varied. The phase $2\pi F_9/H$ is large, typically 6×10^3 at 33 kG, so that a change of F_9 of only 0.1% due to twisting will introduce an extra cycle of oscillation. FM occurs predominantly near [1$\bar{1}$00], where the angular variation of F_9 is most rapid. A quantitative calculation (Ref. 28) shows that a twisting of only 0.04° accounts for the observed FM amplitude, and that the amplitude of P_2 is sufficient to produce such a twist. The alternative explanation for the coupling of F_9 and P_2 through replacement of H by B is inadequate, since the measured amplitude of P_2 is more than two orders of magnitude too small to account for the observed FM amplitude by this mechanism.

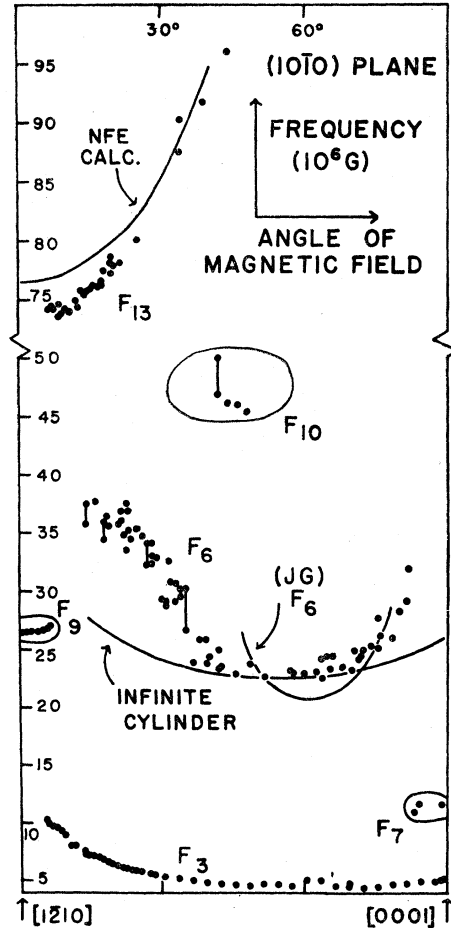[27] The usefulness of this technique was suggested to us by J. H. Condon.

FIG. 5. dHvA frequencies observed for H in the (10$\bar{1}$0) plane. The frequency interval from 50 to 70×10^6 G has been removed as no frequencies were observed in this range.

direction, torque oscillations are observed which go through one complete cycle every time the dHvA frequency changes by H. The angular frequency is thus
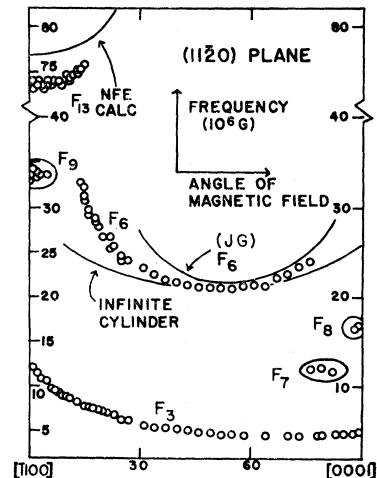

FIG. 6. dHvA frequencies observed for H in the (11$\bar{2}$0) plane. The frequency interval from 40 to 70×10^6 G has been removed as no frequencies were observed in this range.
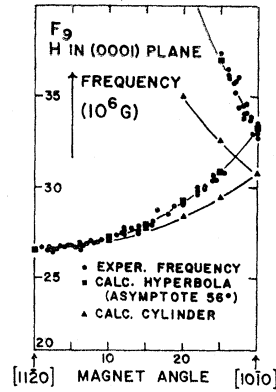
FIG. 7. Frequency F_9 on an expanded scale, compared with calculated frequencies appropriate to a cylindrical Fermi surface and to a hyperbola of revolution with asymptote 56° away from the $[1\bar{2}10]$ axis.

proportional to $dF/d\theta$, and pieces of the Fermi surface with different $dF/d\theta$ can be clearly distinguished. The solid curves of F_9 near $[\bar{1}100]$ (Fig. 4) were obtained by reducing angular oscillations in this manner. The FS segment corresponding to F_9 is hyperboloidal in shape, as seen from Fig. 7 where F_9 is plotted on an expanded scale. For a hyperboloid of revolution, the extremal-area is that area cut by a plane perpendicular to H and passing through the center of symmetry. The dHvA frequency associated with this area varies as[28]

$$F/F_0 = [\cos^2\varphi - (\cotan^2\varphi_0)\sin^2\varphi]^{-1/2}, \qquad (3)$$

where F_0 is the frequency along the $[1\bar{2}10]$ axis of revolution of the hyperboloid, φ is the angle between H and $[1\bar{2}10]$, and φ_0 is the angle of the asymptote of the hyperboloid, at which angle the cross-sectional area goes to infinity. Using the ratio of frequencies $F_{[\bar{1}100]}/F_{[1\bar{2}10]}$, the angle φ_0 was found to be 56°. The solid curve marked "hyperboloid" in Fig. 7 was calculated using this value of φ_0. For comparison, the calculated frequency appropriate to an infinite cylinder is also plotted. As shown in Fig. 7, the upper branch of F_9 disappears 6° away from $[\bar{1}100]$. This disappearance occurs in less than $\frac{1}{2}°$, suggesting the sudden disappearance of the extremal orbit at this critical angle.

F_9 in the $(10\bar{1}0)$ and $(11\bar{2}0)$ Planes

As the magnetic field direction is turned out of the (0001) plane, F_9 becomes unobservable within a few degrees. In the $(11\bar{2}0)$ plane (Fig. 6), it can be followed with some difficulty up to 5° from $[\bar{1}100]$. Owing to the scatter in the data, it is not possible to establish the angular dependence. It was established, however, that F_9 and F_6 in the $(11\bar{2}0)$ plane are not part of the same curve; there is a region of 9° in which neither frequency was observed. In the $(10\bar{1}0)$ plane (Fig. 5), F_9 can be followed up to 6.5° from $[1\bar{2}10]$, turning upward slightly in frequency as its amplitude decreases sharply within $\frac{1}{4}°$ (shown on an expanded scale in Fig. 8).

[28] R. J. Higgins, Ph.D. dissertation, Northwestern University, 1965 (unpublished).

F_{11} [(0001) Plane]

For $H \| [1\bar{2}10]$, this frequency has a value of 48×10^6 G, corresponding to a Fermi surface cross-sectional area of 0.46 Å^{-2}. The amplitude of this oscillation is so small that, even in doubly differentiated data, it shows up as a small modulation of F_9 (upper two curves in Fig. 9). F_{11} is not simply the second harmonic of F_9. At $[1\bar{2}10]$, F_9 is 10% lower than $2F_9$. As H is turned away from $[1\bar{2}10]$, F_{11} decreases slightly whereas F_9 increases.

F_{13} [$(10\bar{1}0)$ and $(11\bar{2}0)$ Planes]

The curves of this frequency are identical in both planes (within the scatter of experimental data), over the range of angles in which the frequency could be resolved. The corresponding Fermi surface is therefore twelvefold symmetric about [0001] for fields near the (0001) plane, and perhaps even cylindrically symmetric. As H approaches the (0001) plane, where this oscillation is least obscured by others, its frequency is 73.5×10^6 G (corresponding to a cross-sectional area of 0.70_2 Å^{-2}) at both the $[1\bar{2}10]$ and $[\bar{1}100]$ directions. This frequency could be followed 17° away from the basal plane in $(11\bar{2}0)$ and 43° in $(10\bar{1}0)$ before becoming obscured because of the large amplitude of F_3 and F_6.

F_{12} [(0001) Plane]

Near $[\bar{1}100]$ this frequency has a value of 71×10^6 G, corresponding to an area of 0.68 Å^{-2}. This oscillation is buried in F_9 and is resolvable only after double differentiation. One of the clearest field sweeps is shown in Fig. 9. It was not possible to conclude whether there is a maximum in frequency at $[\bar{1}100]$ or a crossing of curves with the upper branch of unresolvably small amplitude. It is clear that F_{12} is not the second harmonic of F_9: at $[\bar{1}100]$, $2F_9 = 66 \times 10^6$ G, falling well below F_{12}.

F_{12} in the (0001) plane is so close in frequency to F_{13} in the $(10\bar{1}0)$ and $(11\bar{2}0)$ planes (for $H \perp [0001]$) that they appear at first to be the same orbit. This is somewhat surprising, as the very high symmetry of F_{13} about
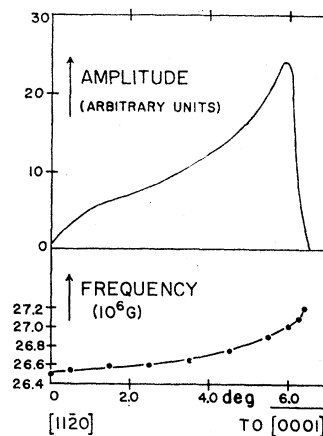

FIG. 8. Angular dependence of amplitude and frequency of F_9 in the $(10\bar{1}0)$ plane for field directions up to 6° from the $[1\bar{2}10]$ axis, showing the sudden disappearance of F_9.
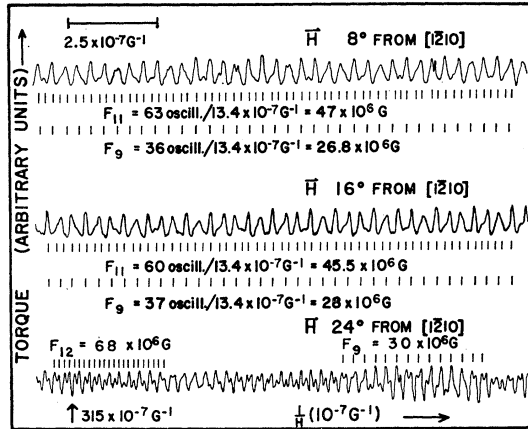
2.5×10⁻⁷G⁻¹   H̄   8° FROM [1̄2̄10]

F_{11} = 63 oscill./13.4×10⁻⁷G⁻¹ = 47×10⁶ G

F_9 = 36 oscill./13.4×10⁻⁷G⁻¹ = 26.8×10⁶ G

H̄ 16° FROM [1̄2̄10]

F_{11} = 60 oscill./13.4×10⁻⁷G⁻¹ = 45.5×10⁶ G

F_9 = 37 oscill./13.4×10⁻⁷G⁻¹ = 28×10⁶ G

H̄ 24° FROM [1̄2̄10]

F_{12} = 68 ×10⁶G F_9 = 30×10⁶G

↑315×10⁻⁷G⁻¹ $\frac{1}{H}$(10⁻⁷G⁻¹) ⟶

(TORQUE (ARBITRARY UNITS))

Fig. 9. Doubly differentiated dHvA oscillations, showing evidence for F_{11} and F_{12} mixed with F_9. The vertical bars under each curve indicate the positions of torque oscillation maxima. F_{11} is seen to distort the shape of F_9 oscillations, while F_{12} shows more clearly pronounced peaks.

[0001] suggests that it would have a negligibly small torque amplitude about a [0001] axis ($\partial F/\partial \theta \simeq 0$). Closer examination shows evidence that F_{12} and F_{13} are not the same orbit. The frequency difference of 2.5×10^6 G is small but more than twice the uncertainty in frequency determination,[29] as shown in Fig. 4. Also, F_{12} was observed only in the vicinity of [1̄100], while F_{13} had nearly equal amplitude near [1̄2̄10] and [1̄100]. It should be pointed out that in a pulsed field measurement, F_{12} would probably be unresolvably small in amplitude compared to F_{13}. This is one of the few cases where the extra term $\partial F/\partial \theta$ in the amplitude of the torsional[3] oscillations aids in the observation of a new frequency.

F_6 [(10 1̄0) and (11 2̄0) Planes]

This oscillation corresponds to the shortest period F_6 measured by JG, but has been resolved with greater clarity[30] as a result of the differentiation technique, not used by JG. Numerical values of F_6 may be summarized as follows:

Plane	F_{min}	θ_{min}	F_α	θ_α	F_β	θ_β
(11 2̄0)	21.0	50	33	14	24	76
(10 1̄0)	22.5	55	37	15	30	82

Here F is in units of 10^6 G; θ_{min} is the angle, $\pm 5°$, at which F_6 is a minimum; θ_α and θ_β are the angles furthest and nearest, respectively, to [0001] at which F_6 can be resolved. It is clear that F_6 corresponds to an orbit on a hyperboloidal sheet of the FS since the frequency rises from its minimum value considerably faster than

[29] The possibility that the small difference between F_{12} and F_{13} was due to long-term drift in the inverse field circuit has been eliminated by measurement of F_{13} in the (10 1̄0) plane both before and after measurement of F_{12} in the (0001) plane. The value of F_{13} was reproducibly larger than that of F_{12}.

[30] A. S. Joseph (private communication).

($1/\cos\theta$) (Figs. 5 and 6). Moreover, the FS sheet is considerably more hyperboloidal in the (10 1̄0) plane than in the (11 2̄0) plane: moving 35° away from θ_0, the frequency increases by 60% and 48%, respectively, from F_0.

F_7, F_8, and F_{10}

These oscillations were very weak compared to F_3, even with double differentiation. F_7 and F_8 were resolved near [0001] at angles where beats occurred between the components of F_3. F_{10} was resolved near the angle where F_3 has a minimum frequency; hence $\partial F/\partial \theta$ is small.

Oscillation	F_7	F_8	F_{10}
Plane	(10 1̄0), (11 2̄0)	(11 2̄0)	(10 1̄0)
Angle from [0001]	5–10°	2°	45°
Frequency (10^6 G)	11–12	17	46
Area (Å⁻²)	0.11	0.16	0.44

ASSIGNMENT OF EXPERIMENTAL AREAS TO THE NEARLY FREE ELECTRON FERMI SURFACE

F_{13}: Lens Orbit

As discussed earlier, the curves of F_{13} in both the (11 2̄0) and (10 1̄0) planes are identical within experimental error. In fact, the symmetry about [0001] may be even higher; if, as discussed earlier, F_{12} is not the same orbit as F_{13}, then no trace of F_{13} was observed for a (0001) torsion axis, leading to the conclusion that there is no detectable asymmetry of F_{13} for magnetic fields in the (0001) plane. Such cylindrical symmetry about [0001] suggests that F_{13} corresponds to the lens orbit, and this is confirmed by a quantitative calculation.[31] In the NFE model, the lens is simply the volume common to the intersection of two spheres centered at points (0000) and (0002). The extremal area A, (which passes through the center of symmetry of the lens) is[28]

$$A(\theta) = 2k^2(\theta)\psi - 2[k_F^2 - b_3^2]^{1/2} b_3 \sin\theta, \qquad (5)$$

where

$$k(\theta) = [k_F^2 - (b_3 \cos\theta)^2]^{1/2}, \qquad (6)$$

and

$$\psi = \cos^{-1}[b_3(\sin\theta)/k(\theta)], \qquad (7)$$

k_F = Fermi sphere radius $= 0.580b_1$ in zinc,

and the angle θ is measured between [0001] and the magnetic field direction. These NFE areas (converted to frequency) are plotted as the solid curve on Figs. 5 and 6. Experimental points lie surprisingly close to the calculated curve. Near [1̄100] and [1̄2̄10], the calculated frequency is 76.8×10^6 G, while the average experimental frequency is slightly lower, at about 73.5×10^6 G, and the difference between experimental and calculated curves is less than 4%. This is closer to the model than indicated by the acoustical measurements of

[31] Calculation of NFEFS extremal areas in hexagonal metals involves the low-temperature axial ratio a_3/a_1. Recent dilatometric measurements to 4.2°K [R. W. Meyerhoff and J. F. Smith, J. Appl. Phys. 33, 219 (1962)] give $a_3/a_1 = 1.830$, or, in k space $b_3/b_1 = 0.473$.

Gibbons and Falicov,[32] who found the lens diameters to be 1.59 Å^{-1} (parallel to [1$\bar{2}$10] and [$\bar{1}$100]) and 0.53 Å^{-1} (parallel to [0001]), which are 13% and 10% smaller, respectively, than the NFE values, giving a lens area 24% smaller than the NFE value for field directions perpendicular to the [0001] direction.

F_9 : Monster Four-Arm Orbit

The main qualitative features of F_9 in the (0001) plane are minimum frequency at [1$\bar{2}$10], hyperboloidal shape, and sudden disappearance 36° from [1$\bar{2}$10]. There is an extremal area which fits these characteristics quite well at the four-arm junction on the monster where two horizontal and two diagonal arms join together.[33] Figure 10 shows this orbit for two angles of the magnetic field in the (0001) plane. Since the extremal area does not pass through a symmetry point, it must be found by an iteration process, constructing NFE sections at various values of k_z (where the z direction is always parallel to H), graphically evaluating orbital area A, and searching for the extremum $\partial A/\partial k_z = 0$. For H parallel to [1$\bar{2}$10], the extremum (a minimum) lies a distance $0.43b_1$ from the center of the zone along the ΓK line, or about three quarters of the distance from Γ to K. The area is 0.32 Å^{-2}, corresponding to a frequency of 34×10^6 G. For H 20° away from [1$\bar{2}$10] in the (0001) plane the extremum lies a distance $0.44b_1$ from Γ and has an area of 0.38 Å^{-2}, corresponding to a frequency of 40×10^6 G. For H closer to [$\bar{1}$100], the orbit becomes elongated along the diagonal arms, and for H 26° away from [1$\bar{2}$10], the orbit no longer closes, running instead into the adjacent zone via the six arm junction at the point H. The vanishing point for this orbit in the NFE model is thus 26° as compared with an experimental value of 36°. However, the effect of the lattice potential on the
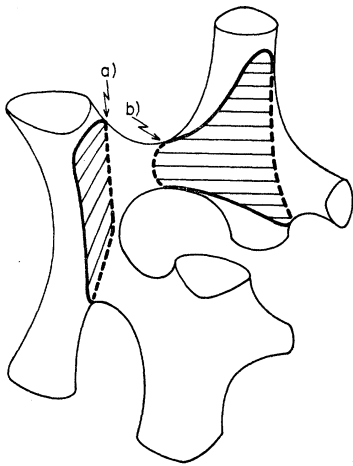
NFE model will be to shrink the six-arm junction and the horizontal arms, and both of these modifications tend to increase the angle at which this orbit vanishes. In fact it is known[8] that the horizontal arms are about a factor of 10 smaller in area than in the NFE model, and, taking the shrinkage to be uniform, this modification alone raises the vanishing angle to 32°, in close agreement with the experimental observation of 36°. Another experimental observation which is well explained by this assignment is the sudden disappearance of F_9 in the (10$\bar{1}$0) plane 6.5° from [1$\bar{2}$10]. As the field is tilted out of the (0001) plane the orbit soon becomes open in the [0001] direction.[34] The observed size of the orbit also corresponds well: the calculated frequency is high by 29% at [1$\bar{2}$10] and by 21% 20° away from [1$\bar{2}$10], suggesting moderate rounding of the corners of the NFE model.

There are several alternative explanations for F_9 which should be considered. There is an orbit around the
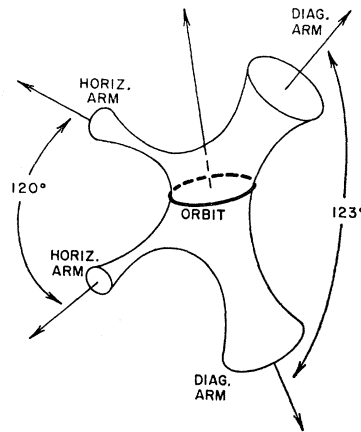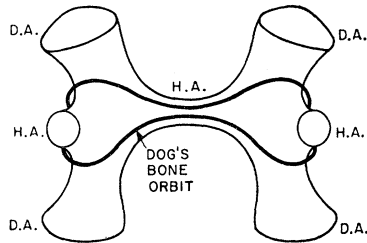

FIG. 11. Monster orbit associated with F_6.

six-arm junction at the point H for magnetic fields near [1$\bar{2}$10]. An examination of the NFE model reveals, however, that the orbit is not planar but bent, and that no planar orbits exist around the six-arm junction. It is not impossible that suitable warping of the monster could produce an orbit around the six-arm junction, but its area would probably be not much more than twice the diagonal arm area at [1$\bar{2}$10], which, experimentally, would be more than a factor of ten too small to account for the frequency of F_9. The alternative possibility that F_9 is connected with orbits on the butterfly will be considered later.

FIG 10. Extremal areas on the second-band monster assigned to the observed frequency F_9. (a) Orbit for $H \| [1\bar{2}10]$. (b) H about 25° from [1$\bar{2}$10]. The area is larger than at (a). For H further away from [1$\bar{2}$10] the orbit becomes open in the [0001] direction.

[32] D. F. Gibbons and L. M. Falicov, Phil. Mag. **8**, 1 (1963).

[33] Real space crystallographic directions of the form ⟨11$\bar{2}$0⟩ are parallel to the edges of the hexagonal face of the Brillouin zone, and the directions ⟨10$\bar{1}$0⟩ are parallel to lines connecting the points Γ and M in the Brillouin zone (Fig. 1).

[34] We have been informed by M. P. Shaw (private communication) that his recent cyclotron mass measurements in zinc include a carrier whose effective mass passes through $0.5m_0$ at about this angle in the (10$\bar{1}$0) plane. If this carrier corresponds to F_9, the amplitude of the dHvA oscillation would vanish because of the term $\cos(\pi m^*/m_0)$ in the Lifshitz formula (Ref. 3). A rough estimate of the effective mass of F_9 near [10$\bar{1}$0] calculated from the temperature dependence of dHvA amplitude is $m^* = (0.5\pm0.1)m_0$, in agreement with Shaw's measurements. However, this interpretation does not fully account for the sudden disappearance of F_9 (Fig. 8).

F_6: Another Four Arm Orbit

Our interpretation of F_6 does not differ from that of JG, who assigned the period P_6 to an orbit on the four-arm junction of the monster. This orbit is shown schematically in Fig. 11 (with the horizontal arms suitably shrunk down to agree with the dHvA area for P_2 obtained by JG). Assignment of this orbit is based on closeness to NFE calculations in size (the experimental area is shrunk down by only about 20% from the NFE area), hyperboloidal angular dependence, and position of minimum frequency about 40° from [0001]. This assignment is also consistent with the observation that the frequency falls to a slightly lower minimum and is less hyperboloidal in the (11$\bar{2}$0) plane than in the (10$\bar{1}$0) plane; in the NFE model, the minimum extremal orbit occurs for a field direction closer to the (11$\bar{2}$0) plane than the (10$\bar{1}$0) plane. Assuming that this identification is correct, some further information about other *dimensions* (as opposed to *areas*) of the Fermi surface can be gained from analysis of the critical angles at which F_6 disappears. As the magnetic field is turned toward the [0001] direction, the disappearance of the

FIG. 13. Alternative monster orbit perhaps associated with F_{12}, arising from magnetic breakdown of the spin-orbit energy gap. The drawing is a section of the NFEFS perpendicular to [$\bar{1}$100] and passing through the center of the zone. Solid and dotted lines are actual spherical sections, while dashed lines are a schematic projection of diagonal arms above and below the plane of the section. In low-magnetic fields, electrons travel open orbits 1291··· and 45674··· and cap orbits 23452··· and 67896····. With magnetic breakdown of the spin-orbit energy gap, an electron travels the orbit 1234567891····.

FIG. 12. Monster orbit perhaps associated with F_{12}, shaped somewhat like a bone. H. A. stands for horizontal arm, D. A. for diagonal arm.

orbit in question depends principally on the height of the horizontal arms. Since the frequency can be followed to within 8° of [0001], it can be shown that the thickness of the horizontal arms in the c direction is less than 0.13 Å^{-1}, or less than 25% of the NFE thickness. Similarly, the disappearance of the orbit near the [$\bar{1}$100] direction is related to the size of the six-arm junction at the point H. A cross section of this junction at the (000$\frac{1}{2}$) plane is roughly an equilateral triangle, and the critical angle for the orbit is related to the length of the side of this triangle. The observation of F_6 within 14° of [$\bar{1}$100] requires that this length be less than 0.12 Å^{-1}, or less than about 60% of the NFE length.

F_{12}: Monster Dog Bone Orbit or Breakdown Orbit

Under the assumption discussed earlier that F_{13} does not appear in a torsion measurement about the [0001] axis, then F_{12} must be assigned to a different piece of the Fermi surface. The only other piece on the NFEFS which is large enough is the monster. There exists an orbit on the monster of roughly the right size, which is shaped rather like a bone, as shown in Fig. 12. The area of this orbit has, qualitatively, the correct angular de-
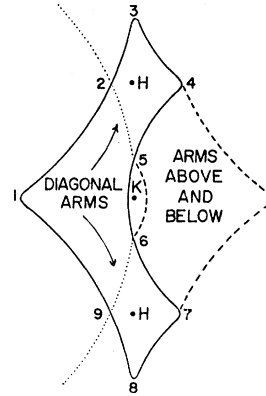
pendence. As the plane of the orbit is tilted away from [$\bar{1}$100], the bone gets slightly longer but much thinner in the middle, resulting in a decrease in area, which is consistent with the behavior of F_{12}. However, this orbit does not have an extremal area required for observation of dHvA oscillations. Taking NFE sections progressively further from the center of the zone, the orbit is first pinched off in the center, then the two halves join together and the area rises monotonically until the orbit becomes open along the diagonal arms. For magnetic fields along [$\bar{1}$100], the corresponding frequency ranges from 46 to 91×10^6 G (observed frequency: 71×10^6 G). The calculated range 5° from [$\bar{1}$100] is 35 to 69×10^6 G (observed frequency: 69×10^6 G). This orbit becomes an extremum if the horizontal arms are pushed in slightly toward the center of the zone. Such warping is not unlikely, as the horizontal arms are not well approximated by the NFEFS. However, this assignment of F_{12} will be regarded as tentative.

There is an alternative assignment of F_{12} which requires magnetic breakdown of the spin-orbit energy gap on the (0001) face, as shown in Fig. 13. Instead of following the open orbit on the monster along the [0001] direction, the electron tunnels through the energy gap and passes over the tip of the cap, then down between the other two monster arms. In the NFEFS, this orbit has an area giving rise to a frequency of 67.5×10^6 G, quite close to F_{12}. Stark[12] has suggested that his magnetoresistance data for this field direction indicates magnetic breakdown of the spin-orbit energy gap for magnetic fields above 17.5 kG, so it is likely that a significant number of electrons would follow this breakdown orbit in the 33 kG magnetic field of the present experiment.

Other Frequencies

F_7, F_8, F_{10} and F_{11} remain to be assigned to orbits on the Fermi surface. Although F_{11} is difficult to resolve experimentally, the observed weak angular dependence (Fig. 4) suggests a piece of the Fermi surface whose cross sectional area is not strongly dependent on the magnetic field direction, falling by only about 5% 20° away from an apparent maximum at $[1\bar{2}10]$. In the NFEFS the first-band caps have a weakly varying cross section but are about 40 times too small to account for a frequency of 47×10^6 G. The only other roughly ellipsoidal segments in the model are the third-band butterflies and the fourth-band cigars. Calculated NFEFS extremal cross sections are shown in Fig. 14, converted to dHvA frequency. The magnitude and angular dependence of the butterfly frequencies in the (0001) plane is somewhat similar to the data in that plane, and suggests an assignment of F_9 alternative to the monster four-arm orbit suggested above. Comparing the butterfly frequencies in the (0001) plane with the data of Fig. 4, one might associate the highest branch with F_{11}, and the middle and lowest branches with upper and lower branches of F_9. Since the butterfly frequencies are about 30% smaller than the observed frequencies, this assignment requires that the lattice potential *increase* the areas, rather than *shrink* them, as is the usual case. However, this is possible in the case of the butterflies, since these surfaces have concave corners where the wings join together, as well as convex corners at the
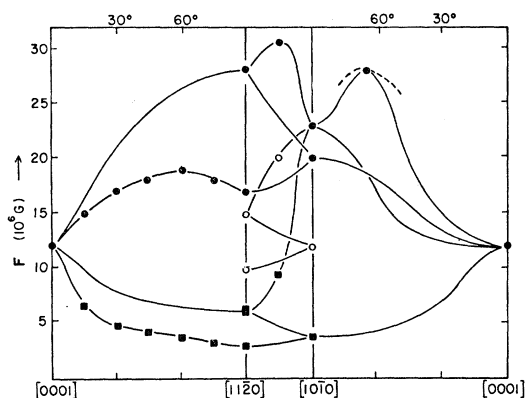

FIG. 14. Calculated NFEFS extremal areas converted to dHvA frequency for the butterfly ● and cigar ○ orbits (single zone scheme) and clamshell orbits ■ in the (0001) plane (double zone scheme). Solid lines are drawn in schematically. By symmetry, each type of segment contributes two extremal areas for H in the $(11\bar{2}0)$ and $(10\bar{1}0)$ planes, and three extremal areas in the (0001) plane. There is a point of contact between butterfly and cigar along the AL line (Fig. 1) causing contact between extremal orbits for H in the $(11\bar{2}0)$ plane. Though orbits slightly displaced from the extrema are separate, this closeness of bands might lead to magnetic breakdown at low fields in the $(11\bar{2}0)$ plane. The butterfly also gives rise to extremal areas which do not pass through the center of symmetry. Such noncentral extrema are required whenever the character of the central extremal area changes from minimum to maximum as the plane of the orbit is rotated. One such noncentral extremum occurs in the $(11\bar{2}0)$ plane near the maximum in the top curves, shown schematically as a dashed curve.

wing tips. To increase the area from the NFE value, the lattice potential would have to round off the concave corners more than the convex corners. This assignment provides a convenient explanation for F_{11}, but there are two strong arguments against assigning F_9 to the butterflies. First, the butterfly orbits do not explain the sudden disappearance of F_9 in the (0001) plane 36° from $[1\bar{2}10]$. Butterfly orbits should also be observable as the field is turned out of the (0001) plane, and in particular do not predict the sudden disappearance of F_9 in the $(10\bar{1}0)$ plane 6.5° away from $[1\bar{2}10]$. Both of these observations suggest rather the disappearance of an extremum on a hyperboloidal orbit at certain critical angles, and favor the interpretation of F_9 discussed above.

Although the angular dependence of F_7 and F_8 has not been established, it seems possible that they correspond to the butterfly and cigar orbits. In the NFEFS model, these frequencies coalesce at [0001] to a value of 12×10^6 G. The lattice potential will split these areas apart at [0001]. Symmetry requires that there be a point of contact between the butterfly and the cigar along the AL line of the Brillouin zone. However, only an infinitesimal number of orbits pass through the point of contact, the majority of orbits still belonging either to the butterfly or to the cigar. The NFE frequency of 12×10^6 G compares well with the experimental values of 12×10^6 G and 17×10^6 G, which we assign tentatively to the butterfly and to the cigar.

The frequency of F_{10} is just twice that of F_6 (within the limited accuracy to which F_{10} could be determined). Although second harmonic oscillations are often resolved in high-pulsed field measurements,[35,36] second harmonics were not observed in any of the present data. However, a value of very nearly $2F_6$ would occur because of a self-intersecting trajectory of the type discussed by Priestley (Ref. 35, Fig. 12, orbit ξ) involving magnetic breakdown onto the needle segment at the point K. The trajectory goes once around the monster orbit of Fig. 11, crosses via the needle onto an equivalent monster orbit in the next band, completing the orbit by crossing back into the initial band via the needle. The frequency due to such an orbit is just $2F_6 - F_1$. Since the frequency F_1 due to the needle is only 0.025×10^6 G at this angle,[10] it is negligible compared to $2F_6 = 46 \times 10^6$ G. Completion of this orbit requires breakdown at two equivalent points on the needle without breakdown at the third. This is not unlikely if the third point is higher on the needle than the other two, since breakdown occurs over a rather narrow region near the center of the needle.[12] However, since F_{10} was only resolved over about 5°, unambigous assignment of F_{10} to the self-intersecting trajectory requires further verification that $F_{10} = 2F_6$ over a wider range of angles.

An alternative assignment of F_{10} may be found on the

[35] M. G. Priestly, Proc. Roy. Soc. (London) **A276**, 258 (1963).
[36] Alexander D. C. Grassie, Phil. Mag. **9**, 847 (1964).

monster in the double-zone scheme. The orbit runs along the length of a diagonal arm, from where the arm joins two horizontal arms up to the corner of the zone. This orbit is closed only in the double-zone scheme; hence it requires magnetic breakdown of the spin-orbit energy gap. The area corresponds to a frequency of about 65×10^6 G, to be compared with observed frequency of 46×10^6 G. Since the diagonal arm in the NFEFS makes an angle of about $30°$ with the $[0001]$ direction, an orbit along it is most likely when H is about $30°$ from the $[\bar{1}100]$ direction, whereas F_{10} is observed with H about $45°$ from $[\bar{1}100]$. However, the observation of F_{10} at this angle is largely a result of F_6 and F_3 becoming small in amplitude at this angle; F_{10} may exist over a larger region of angles.

CONCLUSIONS

Those orbits on the NFEFS which do not depend on whether the single- or double-zone scheme is appropriate are experimentally resolvable over a wide range of angles and correspond well in size to the predictions of the model. In this category are the needle, and the horizontal and diagonal arms of the monster studied by JG. Three of the results from the present investigation are similarly unambiguous. The lens in the largest closed piece of the NFEFS, and one of the pieces not observed by JG. The frequency F_{13} is only 4% smaller than the frequency predicted for the lens orbit when H is perpendicular to $[0001]$. The frequency F_9 is 30% smaller than predicted by the orbit on the monster shown in Fig. 10, which is quite close correspondence in view of the fact that the orbit size is quite sensitive to the lattice potential. The hyperboloidal angular dependence of F_9 is also well approximated by the model, and the $36°$ angular range of F_9 provides correlation of the conclusion[4,8,10] that the horizontal arms of the monster are a factor of 10 smaller in area than predicted by the model. The frequency F_6 is about 20% smaller than predicted by the monster orbit shown in Fig. 11. The angular range of F_6 provides cross correlation of the size of the horizontal arms, and also suggests that the six-arm junction at H is shrunk by 40% in width from the NFEFS.

The sudden disappearance of F_9 $6.5°$ from $[1\bar{2}10]$ as H is tipped out of the (0001) plane is evidence that magnetic breakdown on the monster is far from complete at 33 kG. As long as the monster is connected along the $[0001]$ direction, the extremal orbit to which we have assigned F_9 disappears as H is tipped out of the (0001) plane. Other orbits which could give more direct information concerning magnetic breakdown have not been unambiguously resolved. Frequencies F_7 and F_8 are appropriate in size to the butterflies and cigars, but the experimental angular dependence has not been well enough established to make the assignment definite. In any case these segments are insensitive to breakdown for fields near $[0001]$ where F_7 and F_8 were resolved. Because of the multiplicity of extremal orbits on the monster (eight out of the thirteen frequencies discussed here can be assigned to orbits on this segment) there is ambiguity regarding the assignment of F_{10} and F_{12}. In each case, two orbits were found to be close in area to the observed frequency, one of which required magnetic breakdown of the spin-orbit energy gap.

Until the orientation dependence of frequency has been better established, the interpretation of F_7, F_8, F_{10}, and F_{12} is incomplete, while no interpretation has been found for F_{11}. A system of frequency selective amplification might be more useful than differentiation techniques in the detection of these weak oscillations. It would also be useful in searching for the butterfly, cigar, or clamshell orbits in the (0001) plane, apparently unobserved in this investigation (Fig. 14). Higher fields would be useful in studying F_{10}, F_{11}, and F_{12}. However, since each of these frequencies is near the second harmonic of another frequency, they would be easily obscured by second-harmonic oscillations in high-pulsed field measurements. Furthermore, F_{12} is more appropriately measurable by a torsion method, since it would be obscured by F_{13} in a pulsed field method, as discussed above. However, it is clear that higher field measurements are necessary to track F_{13} above 100 $\times 10^6$ G, and to reveal other higher frequencies; a casual inspection of the ubiquitous monster reveals at least four more extremal orbits larger than those discussed here.